Title: Lineage-dependent variations in single-cell antibiotic susceptibility reveal the selective inheritance of phenotypic resistance within isogenic bacterial populations.

Authors: Wesley Stine [1,#], Tatsuya Akiyama [1,2,#], David Weiss [2,3,4] and Minsu Kim [1,2,4] *

[1] Department of Physics, Emory University, Atlanta, GA, 30322. U.S.A.

[2] Graduate Division of Biological and Biomedical Sciences, Emory University, Atlanta, GA, 30322. U.S.A.

[3] Division of Infectious Diseases, Department of Medicine, Emory University, Atlanta, GA, 30322. U.S.A.

[4]Antibiotic Research Center, Emory University, Atlanta, GA, 30322. U.S.A

# Equal contribution.

* To whom correspondence should be addressed. Tel: 404-727-8037; FAX: 404-727-0873; Email: minsu.kim@emory.edu

Abstract

Research on bacterial resistance to antibiotics has traditionally focused on genetic changes. Yet, even within a population of genetically identical cells, responses to antibiotic exposure are strikingly heterogeneous – some cells succumb while others grow. Here, we investigated the inter-generational propagation of this heterogeneity to understand how bacteria phenotypically adapt to antibiotics. We exposed *Escherichia coli* to the antibiotic breakpoint – the critical concentration used to assess resistance – and tracked cell growth and death at single-cell

resolution in real time. Statistical analysis of the cell survival patterns in the genealogical trees challenged the prevailing notion that the heterogenous response to antibiotics is merely the result of stochastic noise, revealing instead that cell survival depended strongly on the family relationship and age. This dependence led to the enrichment of robust lineages through selective inheritance of resistance factors in an otherwise susceptible population. Mathematical modeling underscores a phenotypically resistant state as a critical ingredient to explain our observation. TolC-mediated efflux, a major factor in multidrug resistance, influences the rates of transition between different states, promoting non-genetic heterogeneity. Our findings establish the presence of 'phenotypic resistance' within a minority population and how it propagates through cell-to-cell heterogeneity. This research has profound implications for pharmacodynamic modeling, single-cell diagnostic technologies for antibiotic resistance, and the broader understanding of resistance mechanisms.

Significance

Bacteria can acquire antibiotic resistance through genetic alterations, a process readily identified by traditional population-level susceptibility tests. However, even genetically identical bacterial cells exhibit heterogeneous responses to antibiotics. In this study, we employed single-cell-resolution imaging, statistical analysis, information theory, and quantitative modeling to characterize this heterogeneity, revealing a non-genetic mechanism of antibiotic resistance. Our findings demonstrate the selective inheritance of phenotypic traits that confer resistance. This advances our understanding of how antibiotic resistance spreads within bacterial populations non-genetically, guides the development of single-cell-level diagnostic technologies for detecting resistance, and informs the design of new treatments that account for phenotypic heterogeneity.

Keyword: Antibiotic resistance, Phenotypic resistance, Phenotypic heterogeneity, Heteroresistance, Efflux pump, TolC, Stochastic modeling.

Introduction

Antibiotics are pivotal in combating bacterial infections but lose their efficacy when administered inappropriately or misused. This problem is further exacerbated by antibiotic-resistant bacteria, which continue to replicate in the presence of antibiotics.

Traditionally, antibiotic resistance was attributed to genetic adaptations, such as mutations and horizontal gene transfer [1]. However, wild-type (WT) bacteria without such genetic adaptations can exhibit resistance, a phenomenon known as intrinsic resistance [1]. A well-documented mechanism for this form of resistance is innate efflux pumps, which extrude antibiotic molecules out of cells [2]. Some of these pumps, notably TolC-Acr tripartite complex, have broad substrate specificity, resulting in the multi-drug resistance phenotype [3]. Recent studies suggest that there are other molecular processes beyond the efflux that likely play significant roles in intrinsic resistance, leading to the proposal of an 'intrinsic resistome' [4].

Antibiotic resistance was commonly characterized using population-averaging techniques. For example, batch-culture optical-density measurements monitor changes in population size. These methods determine the minimum inhibitory concentration (MIC) as a singular metric that assesses the antibiotic susceptibility of an entire population [5]. If the MIC of a strain exceeds the breakpoint concentration of an antibiotic, the strain is categorized as antibiotic-resistant [6]. The MIC is used as an input in pharmacodynamic models to predict the course of antibiotic treatment and develop treatment strategies [7-10].

Over the past decade, it has become clear that genetically-identical cells can exhibit distinct phenotypes [11,12], because molecular processes in the cell are inherently stochastic [13-15]. Notably, gene expression turned out to be 'noisy', which leads to rapid variations in gene product levels within cells, which some studies view as a bet-hedging strategy [11,16].

Similar observations were made in antibiotic treatments of isogenic populations. Despite uniform antibiotic exposure, some cells succumbed and were killed while others replicated [17-21]. This phenomenon was observed broadly for a wide spectrum of antibiotics regardless of their mode of action [22], indicating it is a general principle of bacterial response to antibiotics. However, it is unclear how this cell-to-cell heterogeneity disrupts the population pharmacodynamics. Based on the understanding that stochastic gene expression underlies cell-to-cell heterogeneity, recent studies suggested that the heterogeneity introduces noise to the population dynamics [22-25]. These studies used stochastic branching processes to model cell growth and death under antibiotic exposure as random chance events, predicting rapid population fluctuations. Yet, this perspective overlooks potential regulatory mechanisms that could modulate the heterogeneity to enhance population fitness under antibiotic stress. In particular, if these mechanisms persist near the antibiotic breakpoint, they can manifest as antibiotic resistance, having significant impacts on antibiotic diagnosis tests and treatment strategies [26,27].

In this study, we meticulously examined the heterogeneous response of bacterial cells to antibiotic exposure. Specifically, we exposed an isogenic population of *E. coli* cells to a β-lactam antibiotic (cefsulodin) at its breakpoint concentration and tracked their growth and death at single-cell resolution in real time. We simultaneously traced their family relationship and documented their growth/death patterns in the genealogical trees. We then analyzed these patterns probabilistically using statistical methods, information theory, and quantitative

modeling. The results collectively reveal intricate inheritance dynamics of 'phenotypic resistance' through cell-to-cell heterogeneity, offering novel insights into non-genetic mechanisms underlying antibiotic resistance.

Results

Single-cell-level analysis of cell growth and death

Traditional diagnosis of antibiotic resistance provides an incomplete picture about antibiotic susceptibility. For example, the breakpoint of a β-lactam antibiotic, cefsulodin, is 32 μg/ml [28,29]. A wild-type *E. coli* culture grows to the saturating density at this breakpoint, thereby being categorized as resistant [6] (Fig. 1a; see Supplementary Fig. 1 for growth curve). However, single-cell-level imaging shows that a substantial number of cells are susceptible and are killed at this concentration (Supplementary Movie, left panel). Death of these cells, which occurs concurrently with growth of others, causes the number of live cells in a population to fluctuate dynamically (Fig. 1b). Such population fluctuations have been observed for various other bactericidal drugs [22].

In previous studies, these fluctuations were modeled using a stochastic branching process [22-24]. To test the basis of this modeling, we analyzed the fluctuations in greater depth. Specifically, in addition to counting live cells, we followed the family relationship of these cells, thereby constructing a genealogical tree for each colony. This tree visualizes which cells grew and which died (Supplementary Movie, right panel), displaying the variations in antibiotic susceptibility among individual cells. An experiment encompassing ~30 colonies yielded ~30 genealogical trees, collectively comprising ~4,000 cells. The experiment was independently repeated thrice.

To statistically assess the variations in antibiotic susceptibility, we introduced a survival parameter X. If a cell was susceptible and killed, which is visualized as the termination of the lineage in the tree, we assigned $X = 0$ to the cell. If a cell survived antibiotic exposure and completed the replication (i.e., unsusceptible), $X = 1$ was assigned to the cell. In our genealogical trees, this event is visualized as the split of a lineage.

Cell survival is correlated between kin.

We then quantified how the survival parameter X is correlated between cell pairs with varying degrees of relationship. Conventionally, the degree of relationship refers to the number of generational connections between two individuals. However, this conventional notation is ambiguous. For example, first cousins, great aunts and great nieces all have the degree of four. To uniquely define the relationship, we developed another notation (Fig. 2a). The first number in the square bracket is the number of generations to go up to the common ancestor, and the second is the number to go down to get to the related cell. For example, a first cousin, great aunt and great niece are denoted by [2, 2], [3,1], and [1,3], respectively. The sum of these two numbers equals the conventional degree of connection.

We then performed pairwise Pearson correlation of X for each relationship. The correlation coefficient would be zero if their fates were random. However, our result shows positive correlations (Fig. 2b). This means that if a cell survives, the other cell is more likely to survive as well. The correlation was highest between sibling cells and decreased for more distant relationships (Fig. 2b).

We wondered how the survival correlation changes when a resistance mechanism is inactivated. We inactivated a major antibiotic efflux pump by knocking out *tolC*. The MIC of this mutant fell

below the breakpoint of cefsulodin (Fig. 1a), which underscores the importance of this efflux pump for antibiotic resistance. Because the breakpoint concentration of cefsulodin immediately killed Δ*tolC* cells, we lowered the concentration to 13 μg/ml such that the ratio of growing and dying cells in the Δ*tolC* strain matches that in WT: the mean survival $[X]_{\Delta tolC} = 0.64 \pm 0.04$, which is comparable to $[X]_{WT} = 0.66 \pm 0.01$. Pairwise Pearson correlation analysis again shows positive correlations of survival in the Δ*tolC* strain (Fig. 2c), though the correlation decrease at more distant relationships was more gradual in the Δ*tolC* strain than in the WT strain (Fig. 2b,c). This difference between WT and Δ*tolC* strains will be explored below.

Having analyzed the genealogical tree horizontally above, we next examined the tree vertically. Applying Pearson correlation analysis vertically along the tree is not informative because, for a cell to be present, its direct ancestors (e.g., mother or grandmother) would always have survived antibiotic treatment. Instead, we analyzed how the mean survival [*X*] changes over time as a tree branches out. Due to the binary fission of bacterial cell division, a cell always has an old pole and a newly-formed pole. Upon division, one cell inherits the old pole, carrying on the lineage, while the other receives the new pole. We determined the cell age by the number of generations through which the older pole had been passed down. Previous work offered contradictory predictions about the effects of cell age on fitness. Some studies indicate a decline in fitness with pole age [30,31], while others highlight a preferential accumulation of TolC in older poles, which enhances the fitness of aged cells [32]. We found that [*X*] steadily increased with an increasing cell age for both WT and Δ*tolC* strains (Fig. 2d). Although the Δ*tolC* exhibited a slightly weaker age dependency than WT (the slope in Fig. 2d being 0.0118 ± 0.0033, compared to 0.0168 ± 0.0035 for WT), the difference barely exceeded one standard deviation. This increase in the Δ*tolC* strain

suggests that there are additional resistance factors beyond TolC that accumulate to enhance cell survival.

Inheritance of robust survival

The observed correlation and age-dependence of cell survival suggests the phenotypic inheritance of antibiotic resistance. To further validate this, we characterized cell survival along the lineages. In our analysis, survival refers to a cell that completes its division and produces two daughter cells (D). However, if only one daughter cell survives antibiotic treatment ($D = 1$) or none survive ($D = 0$), the mother cell's survival does not contribute to overall population growth. Here, we categorized survival of a cell as *robust* if both of its daughter cells survived ($D = 2$). When we identified the robust mother cells in our dataset and determined their frequency, $F(\mathrm{R}_{N=1})$, we found that these robust cells were present more frequently than expected by random chance, $F_0(\mathrm{R}_{N=1})$; see Supplementary Fig. 2. The relative frequency, i.e., the ratio of $F(\mathrm{R}_{N=1})$ and $F_0(\mathrm{R}_{N=1})$, was plotted in Fig. 3a. Here, N=1 refers to the fact that only one generation was considered.

To examine the heritability of robust survival, we next assessed how likely daughter cells are robust when their mother cell is robust. This was quantified by the conditional probability, $P\,(D = 2 \mid \mathrm{R}_{N=1})$, i.e., the probability of two daughter cell survival ($D = 2$) conditioned upon one generation of robustness ($\mathrm{R}_{N=1}$). As shown in Fig. 3b (left column), this conditional probability was higher than the non-conditional probability: $P\,(D = 2)$ denoted by a dash line in Fig. 3b. This observation suggests that robust survival is heritable from generation to generation.

Enrichment of robust lineages

This heritability was more pronounced when we considered multiple generations. We first predicted that the positive effect of robust mothers on daughter cells would elevate the frequency of two consecutive generations exhibiting robustness, denoted as $F(R_{N=2})$. Indeed, this frequency was much higher than the frequency expected by random chance, $F_0(R_{N=2})$, with a fold difference greater than that observed for one generation of robustness (Fig. 3a and Supplementary Fig. 2). We also found that the daughter cells originating from the two robust generations are more likely to be robust than daughter cells from one robust generation; $P(D = 2| R_{N=2}) > P(D = 2| R_{N=1})$, as shown in Fig. 3b. This trend continued for three consecutive generations of robustness ($N = 3$), which were even more over-represented than expected by random chance, with a fold change greater than that observed for two robust generations (Fig. 3a). Moreover, daughter cells originating from three robust generations exhibited an even higher likelihood of robust survival compared to those from two generations. (Fig. 3b). These data indicate positive feedback on robust lineages, where robust lineages become progressively more likely to produce robust offspring, thereby increasing their representation in the population.

We additionally found that once cells 'ride the tide' to produce robust lineages, these lineages are less likely to go extinct. This effect was uncovered when we analyzed how likely a robust cell give birth to non-robust cells. Here, being non-robust means either one of their daughter cells die, $D = 1$ (Supplementary Fig. 3, right panel) or both dies $D = 0$ (Fig. 3c), with the latter indicating the termination of the lineage branch. We observed a decreasing probability of the termination with each additional generation of robustness (Fig. 3c). This highlights a trend where robust lineages are more likely to persist and propagate.

We made contrasting observations when we investigated the fate of non-robust lineages, particularly the extreme case where there is only a single surviving line, and all other cells die in

196 the lineage (Supplementary Fig. 4a diagram). We found that these non-robust lineages are much
197 less likely to produce robust daughter cells (Supplementary Fig. 4a). Instead, these daughter cells
198 are much more likely to die (Supplementary Fig. 5a), meaning the lineages that failed to exhibit
199 robustness were more likely to terminate.

200 There are two potential mechanisms for the observed propagation of robust lineages: (i)
201 accumulation of resistance factors or (ii) decrement of antibiotic-induced cellular damage. Either
202 of these mechanisms can explain the observed increase in the conditional probability of robust
203 daughter cells with an increasing number of robust generations. We therefore analyzed how an
204 increasing number of non-robust generations affects the conditional probabilities of daughter cell
205 survival ($D = 2$, $D = 1$, and $D = 0$). Surprisingly, we found that these probabilities changed little
206 with the number of non-robust generations, showing a plateau (Supplementary Fig. 3-5). This
207 plateau indicates that cellular damage by antibiotics is constant, supporting the accumulation of
208 resistant factors.

209 The lineages we analyzed above represent two extreme patterns of ancestral history (either all
210 cells survive or die). In the population, however, there are other possible combinations of
211 ancestral survival (e.g., an aunt survives but one cousin dies, etc.). Here, we sought to analyze
212 how daughter cells originating from different ancestral combinations survive differently to gain
213 insight into the inheritance of resistance across the population. Because we recorded the fate of
214 every cell in our dataset, we can explore this relationship for each combination of ancestral
215 history. However, the diversity of these combinations is vast; for instance, within just three
216 generations of an ancestral lineage, up to eighty different combinations of cell fate are possible.
217 To manage this complexity and extract meaningful insights about the inheritance, we turned to
218 information theory. Briefly, we used Shannon entropy to quantify the uncertainty, i.e., missing

information in predicting the fates of two daughter cells, $H(M)$. We then determined how this uncertainty changes when incorporating the knowledge of ancestral survival Y_N. The reduction in the entropy, $H(M) - H(M|Y_N)$, widely known as mutual information [33], reveals how much information ancestral survival history provides to the fates of daughter cells. This analysis showed that, in WT, the information content remains relatively constant across multiple generations (Fig. 3d), meaning that at the population level, the survival of daughter cells is minimally influenced by their lineage history. This finding appears to contrast with the pronounced lineage-dependent dynamics of robustness we identified earlier, where robust lineages exhibited a clear pattern of inherited resistance. This contrast indicates that the resistance inheritance that confers advantages to robust lineages is unique to these lineages and does not uniformly apply across the entire population.

Minimal requirement for a quantitative model.

We next sought to develop a minimum model to explain key aspects of our data. Previously, we and others tested a two-state Markov chain model where a cell survives or dies randomly during antibiotic exposure [22-24]. While this model can explain heterogeneous response of cells to antibiotics, it fundamentally assumes no correlation in these responses between cells. However, we observed the kinship correlation (Fig. 2b,c). Importantly, this correlation is central to lineage-dependent response to antibiotic exposure. To construct a model that generates the kinship correlation, we incorporated the phenomenon of robust survival observed in our experiments into the model, introducing a 'phenotypically healthy' state (Fig. 4a). Cells in this state give rise to daughter cells equipped to withstand antibiotic exposure, and thus both daughter cells survive. Conversely, while a phenotypically "vulnerable' cell can still divide, its daughter cells might succumb to antibiotic exposure, entering a 'dead' state. In our model, daughter cells can either

preserve the same state as their mothers or shift to an adjacent state. For example, healthy mother cells might yield healthy daughter cells or produce vulnerable ones due to antibiotic damage. A vulnerable mother cell could produce either vulnerable or dead daughter cells, or it could recover from the damage, giving birth to healthy daughter cells. This three-state Markov chain is summarized in Fig. 4a.

The major difference of this model from the two-state model is that it predicts the cell fate correlation. Specifically, the healthy mother cells produce two surviving daughter cells, resulting in sibling correlation. If these daughter cells have a higher-than-average probability of sharing the mother's healthy state, then the correlation will occur at more distant relationships. This long-lasting correlation will manifest as the propagation of robust survival. The numerical simulation shows that this model quantitatively explains the observed pattern of survival correlation (Fig. 2bc, line). The fit of the model reveals the rate of transition between different states (Fig. 4b). It is plausible that cells' response could be modeled better with more than three states, which we plan to test in our future studies. However, our model convincingly demonstrates that a three-state model is sufficient to explain the broad correlation pattern that we observed.

We then compared the parameter values for WT and Δ*tolC* strains to gain molecular insights into the quantitative mechanism described above. As mentioned above, TolC contributes significantly to antibiotic resistance (Fig. 1a). We therefore had to reduce the cefsulodin concentration for the Δ*tolC* strain so that its mean survival [*X*] was comparable to that of WT at the breakpoint. This explains why the killing rates are comparable between WT and Δ*tolC* strains (Fig. 4b). However, the recovery rate of the Δ*tolC* strain was one order of magnitude lower than that of WT (Fig. 4b).

To understand this difference, we considered the molecular function of TolC. It is a major component for the efflux pump, which lowers the intracellular antibiotic concentration. While WT cells experience more damage (Fig. 4b, presumably because they are exposed to a higher antibiotic concentration), they also exhibit a higher recovery rate, leading to frequent transition between states. Interestingly, recent studies found that the expression of TolC, as well as Acr which forms a complex with TolC to extrude antibiotics, is stochastic [34-37], providing a potential molecular mechanism for this frequent transition. On the other hand, because Δ*tolC* exhibits the lower rates of damage and recovery, cells maintain their phenotypic states longer, which will lead to higher survival correlation between distantly related cells (Fig. 2b,c). The long-lasting correlation results in stronger lineage-dependent dynamics of robustness (Fig. 3bc) and higher information content in ancestral history (Fig. 3d) in the Δ*tolC* compared to WT.

Discussion

Antibiotic susceptibility is characterized by how a population of bacteria as a whole responds to antibiotics. Heterogeneous responses of isogenic cells therefore complicates antibiotic diagnostic tests and treatments [26,27]. In particular, the survival of small subpopulations can lead to antibiotic treatment failure and recurrence of infections. Here, we meticulously characterized heterogeneous cell growth and death under antibiotic exposure. We first observed that antibiotic-exposed populations exhibit seemingly random population fluctuations (Fig. 1), consistent with previous findings [22]. When we recorded cell growth and death in genealogical trees and analyzed their pattern probabilistically, we observed intricate trends. Cell survival was not random but correlated among kin (Fig. 2). Robust cells produce robust offspring, thereby enriching the robust lineages (Fig. 3). This robustness further strengthened across the generations, indicating phenotypic adaptation to antibiotics (Fig. 3). This positive feedback was due to the inheritance of

resistance factors whereas antibiotic-induced cellular damage remained constant. Information theory indicates that this inheritance is unique to the robust lineages and is obscured in the population-level analysis (Fig. 3d), highlighting a challenge in studying this phenomenon using a population-averaging approach. Based on the analysis of robust lineages, we developed a quantitative model that includes a phenotypically healthy state, articulating the minimum ingredient to explain our data (Fig. 4). Additional analysis of the Δ*tolC* strain shows that antibiotic efflux alters the rates of transition between different states, thereby amplifying cellular heterogeneity (Fig. 4). Collectively, our findings demonstrate intricate dynamics of phenotypic resistance that propagates selectively in a minority population, offering novel insights into non-genetic mechanisms underlying antibiotic resistance.

We believe our findings are particularly timely, aligning with the intense interests in advancing single-cell-level antibiotic susceptibility diagnosis. The past few years have witnessed a significant rise in cutting-edge approaches, which leverage microfluidics and microdroplets in combination with optical, electrochemical, or isothermal techniques to measure the mass, size, and morphology of single cells exposed to antibiotics [38-41]. These new developments will greatly facilitate the thorough quantitative analyses demonstrated here. In parallel, our findings can guide the refinement and application of these techniques to fulfill their potential. For example, measuring bacterial responses to antibiotics over multiple generations is critical to evaluate phenotypic resistance. The dynamics of cell growth and death can be analyzed quantitatively to deduce the rates of transition into and out of the resistance state. Such detailed knowledge will provide a more complete view of population dynamics under antibiotic exposure, advancing our understanding of pharmacodynamics, which will improve antibiotic treatments. Another exciting development in the field is “single-cell” omic techniques, which are rapidly improving to

decrease the number of bacterial cells needed to make transcriptomic and proteomic measurements [42,43]. Focusing these techniques on the robust lineages can reveal the differential molecular profiles that underlie the inheritance of phenotypic resistance.

Method

Experimental Procedure

Bacterial strains and growth conditions.

E. coli K-12 NCM3722 [44-46] and its Δ*tolC* derivative (NMK320)[47] were grown in LB broth (Miller) supplemented with 10 mM glucose and 1 mM $MgSO_4$. Briefly, a single colony was inoculated into media in borosilicate glass culture tubes and incubated at 37°C with shaking (250 rpm) in a water bath shaker overnight. Next morning, the culture was diluted with fresh media to optical density (OD_{600}) of ~0.001 and incubated in a water bath shaker at 37°C with shaking.

Time lapse imaging of bacterial growth.

Time lapse microscopy was performed as previously described [48,49]. When a cell culture reached OD_{600} > 0.05, cells were placed on a 35 mm glass bottom petri dish (Cellvis) and covered with a 1.5 % agarose pad containing LB, 10 mM glucose, 1 mM $MgSO_4$, and cefsulodin. Cells were imaged every 5 minutes using an inverted fluorescence microscope (Olympus IX83) with an oil immersion phase-contrast 60× objective seated inside an incubator chamber (InVivo Scientific) pre-warmed to 37°C. The microscope was controlled with MetaMorph software (Molecular Devices).

Wild-type cells were grown with a cefsulodin concentration 31 μg/mL and the Δ*tolC* mutant with 13 μg/mL. A total of 91 WT colonies (37 living and 54 extinct) and 112 Δ*tolC* colonies (38

331 living and 74 extinct) were analyzed. In these colonies we had a total of 12,512 WT cells and
332 14,866 Δ*tolC* cells.

333 **Image analysis.**

334 Cell tracking.

335 Cell division and location of cells were tracked using a TrackMate v7.10.2, a plug-in of Fiji,
336 ImageJ [50] Cefsulodin induces a variety of cell shapes [51]. Instead of segmenting the cells, we
337 simply tracked the birth and location of cell poles at each time frame. Marked cell poles of the
338 same cell in different frames were linked, and old poles of newborn cells were linked to their
339 parents, so that genealogical trees could be constructed. We marked the moment of death when
340 cells are visibly lysed or permanently arrested their growth. Cells were tracked until either a
341 whole population went extinct, or the field became so crowded that individual cells could not be
342 reliably distinguished. We then assigned a unique identification to each cell representing the age
343 of the cell pole, generation, and kinship; see Supplementary Fig. 6 for detail.

344 Statistical analyses

345 The Pearson correlation coefficient for two datasets is a number between -1 and +1 that measures
346 the correlation between them. For a dataset of size N in which each datapoint is represented by
347 two variables, x and y, the correlation coefficient is given by

348 $$C = \frac{\sum_{i=1}^{N}(x_i - \bar{x})(y_i - \bar{y})}{\sqrt{\sum_{i=1}^{N}(x_i - \bar{x})^2}\sqrt{\sum_{i=1}^{N}(y_i - \bar{y})^2}}$$

349 In order to account for potential experimental bias that might produce correlation, we determined
350 the 'background correlation'. Background cells were born in the same colony as the primary

cells, in either the same or an adjacent frame, but separated by seven or more degrees of kinship. We found that the correlation coefficients between the primary cells and the background cells, C_B, were very close to zero, indicating no significant experimental bias. For extra caution, we subtracted the background correlation from the above calculated correlation C as follows,

$$C_{net} = \frac{C - C_B}{1 - C_B}.$$

The subtracted values are plotted in Fig. 2bc.

Three-state Markov model

Details of the model construction were provided with equations in Supplementary Note.

Shannon entropy calculation

Shannon entropy is defined as $H(M) \equiv -\sum p_M \log_2 p_M$, where M refers to different microstates for the fates of two daughter cells, i.e. both survive, elder survives, younger survives, and both die. Because we know the fates of every cell, we can calculate the probability of each microstate (p_M) and hence Shannon entropy. We then calculated Shannon entropy conditioned upon the fates of cells in the prior generation: $H(M|Y) \equiv \sum p_y H(M|Y = y)$. For example, the Shannon entropy conditioned upon the fates of the '1' generations was calculated in the following way:

$$H(M|X_{aunt}) = p(X_{aunt} = 1)H(M|X_{aunt} = 1) + p(X_{aunt} = 0)H(M|X_{aunt} = 0).$$

The difference between the original and conditional Shannon entropy is equal to mutual information, which is plotted in Fig. 3d. We corrected the potential bias due to small sample size by using Miller-Madow correction [52].

Acknowledgements

371 This work was funded by NIH (1U19AI158080), MP3 Initiative (00097584) and Keck
372 foundation (0000070212). We thank Stefan Boettcher, Daniel Weissman, and all the lab
373 members for helpful discussions. We thank Jing Yan and JC Gumbert for the critical reading of
374 the manuscript and for providing feedback.

375 **Author Contributions.**

376 TA, and MK conceived the study. TA designed the experiments. WS and TA analyzed and
377 interpreted the data. DW provided feedback. DW and MK secured funding and provided
378 resources. TA and MK wrote the manuscript. All authors read and approved the manuscript.

379 **Competing Interests**

380 Authors declare no competing interests.

381 **Data Availability Statements**

382 The datasets are provided as Supplementary Data.

383

384 **Figure Caption**

385 **Fig. 1. Growth of *E. coli* exposed to cefsulodin.**

386 a). Images of wild type and Δ*tolC* cultures after 24 hours of incubation with different
387 concentrations of cefsulodin. See Supplementary Fig. 1 for growth curves. The experiment was
388 repeated twice and similar images were obtained. b). Representative growth of wild-type cells
389 exposed to the breakpoint concentration of cefsulodin. We inoculated multiple *E. coli* colonies
390 on solid media containing the breakpoint concentration of cefsulodin and counted the number of
391 live cells in ~30 colonies. The number of live cells from 4 colonies is shown here as an example.

Different colors indicate different colonies. Two additional biological replicates were performed, and similar population fluctuations were observed.

Fig. 2. Cell survival is correlated.

a) Labeling scheme of relationship. The first number in the square bracket is the number of generations to go up to a common ancestor, and the second is the number to go down to get to the related cell. The sum of these two numbers is equal to the conventional degree of separation. b and c). Pearson correlation of the survival parameter, X, for WT and Δ*tolC* strains. The lines are from the model fit; see Fig. 4 for the model. d) We sorted cells according to the lineage age and calculated the mean survival [X]. The slope of this increase was 0.0168 ± 0.0035 for WT cells, and 0.0118 ± 0.0033 for the Δ*tolC* strain. Small open circles indicate the raw data from three biological replicates. The columns and solid circles indicate their means. To calculate the error bar, we compared the standard deviation of raw data from three biological repeats and the standard error for a binomial distribution with the number of cell pairs used and plotted whichever was larger.

Fig. 3. The propagation of lineage-dependent survival.

In our analysis, survival refers to a cell that completes its division and produces two daughter cells (D). Both of these daughter cells might be killed by antibiotic treatment before their own division (D = 0), one daughter cell might survive (D = 1), or both might survive (D = 2). The latter is categorized as robust survival. (a). We identified the robust mother cells in our dataset, determined their frequency, $F(R_{N=1})$ and compared it with what would be expected by random chance, $F_0(R_{N=1})$. The relative difference is plotted here. See Supplementary Fig. 2 for raw data. We then determined the frequency for two consecutive generations of robustness $F(R_{N=2})$, i.e.,

robust grandmother, mother, and aunt. The frequency for three consecutive generations of robustness $F(R_{N=3})$ was determined in a similar manner. (b). We calculated the conditional probability, i.e., probability that daughter cells are robust given (i) their mother cell was robust $R_{N=1}$, (ii) two generations of robustness $R_{N=2}$, and (iii) three generations of robustness, $R_{N=3}$. The dash line refers to the non-conditional probability $P\ (D = 2) = X^2$. c). Conditional probability that both daughter cells die ($D = 0$) given different generations of robustness. d) Information stored in the ancestral survival history. Red (left) and green (right) columns indicate WT and Δ*tolC* strains, respectively. The columns represent the values obtained by combining data from all three independent experiments. The error bar represents the standard error calculated using the values from three biological repeats.

Fig. 4. A minimal model to explain the survival correlation and inheritance.

a) The previous two-state Markov model cannot explain the survival correlation. We introduced a phenotypically healthy state into this model to account for robust survival. b) We fit the data (lines in Fig. 2bc) with this model to determine the transition rates. Small open circles show the rates determined for three independent experiments. The columns and error bar indicate the means and standard deviation from the independent experiments.

Reference

1 Blair, J. M. A., Webber, M. A., Baylay, A. J., Ogbolu, D. O. & Piddock, L. J. V. Molecular mechanisms of antibiotic resistance. *Nat Rev Micro* **13**, 42-51 (2015). https://doi.org:10.1038/nrmicro3380

2 Nikaido, H. & Pagès, J.-M. Broad-specificity efflux pumps and their role in multidrug resistance of Gram-negative bacteria. *FEMS microbiology reviews* **36**, 340-363 (2012). https://doi.org:10.1111/j.1574-6976.2011.00290.x

3 Kobylka, J., Kuth, M. S., Müller, R. T., Geertsma, E. R. & Pos, K. M. AcrB: a mean, keen, drug efflux machine. *Annals of the New York Academy of Sciences* **1459**, 38-68 (2020). https://doi.org:https://doi.org/10.1111/nyas.14239

4 Cox, G. & Wright, G. D. Intrinsic antibiotic resistance: Mechanisms, origins, challenges and solutions. *International Journal of Medical Microbiology* **303**, 287-292 (2013). https://doi.org:https://doi.org/10.1016/j.ijmm.2013.02.009

5 Andrews, J. M. Determination of minimum inhibitory concentrations. *The Journal of antimicrobial chemotherapy* **48 Suppl 1**, 5-16 (2001).

6 Turnidge, J. & Paterson, D. L. Setting and revising antibacterial susceptibility breakpoints. *Clin Microbiol Rev* **20**, 391-408, table of contents (2007). https://doi.org:10.1128/cmr.00047-06

7 Craig, W. A. Pharmacokinetic/Pharmacodynamic Parameters: Rationale for Antibacterial Dosing of Mice and Men. *Clinical Infectious Diseases* **26**, 1-12 (1998). https://doi.org:10.1086/516284

8 Regoes, R. R. *et al.* Pharmacodynamic Functions: a Multiparameter Approach to the Design of Antibiotic Treatment Regimens. *Antimicrob. Agents Chemother.* **48**, 3670-3676 (2004). https://doi.org:10.1128/aac.48.10.3670-3676.2004

9 Falagas, M. E., Tansarli, G. S., Rafailidis, P. I., Kapaskelis, A. & Vardakas, K. Z. Impact of Antibiotic MIC on Infection Outcome in Patients with Susceptible Gram-Negative Bacteria: a Systematic Review and Meta-Analysis. *Antimicrob. Agents Chemother.* **56**, 4214-4222 (2012). https://doi.org:10.1128/aac.00663-12

10 Czock, D., Markert, C., Hartman, B. & Keller, F. Pharmacokinetics and pharmacodynamics of antimicrobial drugs. *Expert Opinion on Drug Metabolism & Toxicology* **5**, 475-487 (2009). https://doi.org:10.1517/17425250902913808

11 Ackermann, M. A functional perspective on phenotypic heterogeneity in microorganisms. *Nat Rev Micro* **13**, 497-508 (2015). https://doi.org:10.1038/nrmicro3491

12 Balazsi, G., van Oudenaarden, A. & Collins, J. J. Cellular decision making and biological noise: from microbes to mammals. *Cell* **144**, 910-925 (2011). https://doi.org:10.1016/j.cell.2011.01.030

13 Choi, P. J., Cai, L., Frieda, K. & Xie, X. S. A Stochastic Single-Molecule Event Triggers Phenotype Switching of a Bacterial Cell. *Science* **322**, 442-446 (2008). https://doi.org:10.1126/science.1161427

14 Swain, P. S., Elowitz, M. B. & Siggia, E. D. Intrinsic and extrinsic contributions to stochasticity in gene expression. *Proceedings of the National Academy of Sciences of the United States of America* **99**, 12795-12800 (2002). https://doi.org:10.1073/pnas.162041399

15 Vashistha, H., Kohram, M. & Salman, H. Non-genetic inheritance restraint of cell-to-cell variation. *eLife* **10**, e64779 (2021). https://doi.org:10.7554/eLife.64779

16 Veening, J. W., Smits, W. K. & Kuipers, O. P. Bistability, epigenetics, and bet-hedging in bacteria. *Annual review of microbiology* **62** (2008). https://doi.org:10.1146/annurev.micro.62.081307.163002

17 Balaban, N. Q. *et al.* Definitions and guidelines for research on antibiotic persistence. *Nature Reviews Microbiology* **17**, 441-448 (2019). https://doi.org:10.1038/s41579-019-0196-3

18 El-Halfawy, O. M. & Valvano, M. A. Antimicrobial Heteroresistance: an Emerging Field in Need of Clarity. *Clinical Microbiology Reviews* **28**, 191-207 (2015). https://doi.org:10.1128/cmr.00058-14

19 Dewachter, L., Fauvart, M. & Michiels, J. Bacterial Heterogeneity and Antibiotic Survival: Understanding and Combatting Persistence and Heteroresistance. *Mol. Cell* **76**, 255-267 (2019). https://doi.org:https://doi.org/10.1016/j.molcel.2019.09.028

20 Akiyama, T. & Kim, M. Stochastic response of bacterial cells to antibiotics: its mechanisms and implications for population and evolutionary dynamics. *Current opinion in microbiology* **63**, 104-108 (2021). https://doi.org:https://doi.org/10.1016/j.mib.2021.07.002

21 Brandis, G., Larsson, J. & Elf, J. Antibiotic perseverance increases the risk of resistance development. *Proceedings of the National Academy of Sciences* **120**, e2216216120 (2023). https://doi.org:doi:10.1073/pnas.2216216120

22 Coates, J. *et al.* Antibiotic-induced population fluctuations and stochastic clearance of bacteria. *eLife* **7**, e32976 (2018). https://doi.org:10.7554/eLife.32976

23 Teimouri, H. & Kolomeisky, A. B. Theoretical investigation of stochastic clearance of bacteria: first-passage analysis. *Journal of The Royal Society Interface* **16**, 20180765 (2019). https://doi.org:doi:10.1098/rsif.2018.0765

24 Marrec, L. & Bitbol, A.-F. Resist or perish: Fate of a microbial population subjected to a periodic presence of antimicrobial. *PLoS computational biology* **16**, e1007798 (2020). https://doi.org:10.1371/journal.pcbi.1007798

25 Alexander, H. K. & MacLean, R. C. Stochastic bacterial population dynamics restrict the establishment of antibiotic resistance from single cells. *Proceedings of the National Academy of Sciences* **117**, 19455-19464 (2020). https://doi.org:10.1073/pnas.1919672117

26 Andersson, D. I., Nicoloff, H. & Hjort, K. Mechanisms and clinical relevance of bacterial heteroresistance. *Nature Reviews Microbiology* **17**, 479-496 (2019). https://doi.org:10.1038/s41579-019-0218-1

27 Band, V. I. & Weiss, D. S. Heteroresistance: A cause of unexplained antibiotic treatment failure? *PLoS pathogens* **15**, e1007726 (2019). https://doi.org:10.1371/journal.ppat.1007726

28 Statement 1996 CA-SFM Zone sizes and MIC breakpoints for non-fastidious organisms. *Clinical Microbiology and Infection* **2**, S46-S49 (1996). https://doi.org:10.1111/j.1469-0691.1996.tb00875.x

29 Thibault, F. M., Hernandez, E., Vidal, D. R., Girardet, M. & Cavallo, J.-D. Antibiotic susceptibility of 65 isolates of Burkholderia pseudomallei and Burkholderia mallei to 35 antimicrobial agents. *J. Antimicrob. Chemother.* **54**, 1134-1138 (2004). https://doi.org:10.1093/jac/dkh471

30 Proenca, A. M., Rang, C. U., Buetz, C., Shi, C. & Chao, L. Age structure landscapes emerge from the equilibrium between aging and rejuvenation in bacterial populations. *Nature communications* **9**, 3722 (2018). https://doi.org:10.1038/s41467-018-06154-9

31 Proenca, A. M., Rang, C. U., Qiu, A., Shi, C. & Chao, L. Cell aging preserves cellular immortality in the presence of lethal levels of damage. *PLOS Biology* **17**, e3000266 (2019). https://doi.org:10.1371/journal.pbio.3000266

32 Bergmiller, T. *et al.* Biased partitioning of the multidrug efflux pump AcrAB-TolC underlies long-lived phenotypic heterogeneity. *Science* **356**, 311-315 (2017). https://doi.org:10.1126/science.aaf4762

33 Thomas M. Cover, J. A. T. in *Elements of Information Theory* Ch. 2, 13-55 (John Wiley & Sons, Inc., 2005).

34 El Meouche, I., Siu, Y. & Dunlop, M. J. Stochastic expression of a multiple antibiotic resistance activator confers transient resistance in single cells. *Scientific reports* **6**, 19538 (2016). https://doi.org:10.1038/srep19538

35 Krishnamoorthy, G., Tikhonova, E. B., Dhamdhere, G. & Zgurskaya, H. I. On the role of TolC in multidrug efflux: the function and assembly of AcrAB-TolC tolerate significant depletion of intracellular TolC protein. *Molecular microbiology* **87**, 982-997 (2013). https://doi.org:10.1111/mmi.12143

36 Łapińska, U. *et al.* Fast bacterial growth reduces antibiotic accumulation and efficacy. *eLife* **11**, e74062 (2022). https://doi.org:10.7554/eLife.74062

37 Guet, C. C., Bruneaux, L., Oikonomou, P., Aldana, M. & Cluzel, P. Monitoring lineages of growing and dividing bacteria reveals an inducible memory of mar operon expression. *Frontiers in Microbiology* **14** (2023). https://doi.org:10.3389/fmicb.2023.1049255

38 Kadlec, M. W., You, D., Liao, J. C. & Wong, P. K. A Cell Phone-Based Microphotometric System for Rapid Antimicrobial Susceptibility Testing. *J Lab Autom* **19**, 258-266 (2014). https://doi.org:10.1177/2211068213491095

39 Etayash, H., Khan, M. F., Kaur, K. & Thundat, T. Microfluidic cantilever detects bacteria and measures their susceptibility to antibiotics in small confined volumes. *Nature communications* **7**, 12947 (2016). https://doi.org:10.1038/ncomms12947

40 Sinn, I. *et al.* Asynchronous magnetic bead rotation (AMBR) biosensor in microfluidic droplets for rapid bacterial growth and susceptibility measurements. *Lab Chip* **11**, 2604-2611 (2011). https://doi.org:10.1039/c0lc00734j

41 Baltekin, Ö., Boucharin, A., Tano, E., Andersson, D. I. & Elf, J. Antibiotic susceptibility testing in less than 30 min using direct single-cell imaging. *Proceedings of the National Academy of Sciences* **114**, 9170-9175 (2017). https://doi.org:doi:10.1073/pnas.1708558114

42 Ma, P. *et al.* Bacterial droplet-based single-cell RNA-seq reveals antibiotic-associated heterogeneous cellular states. *Cell* **186**, 877-891.e814 (2023). https://doi.org:10.1016/j.cell.2023.01.002

43 Baysoy, A., Bai, Z., Satija, R. & Fan, R. The technological landscape and applications of single-cell multi-omics. *Nature Reviews Molecular Cell Biology* **24**, 695-713 (2023). https://doi.org:10.1038/s41580-023-00615-w

44 Brown, S. D. & Jun, S. Complete Genome Sequence of Escherichia coli NCM3722. *Genome Announcements* **3** (2015). https://doi.org:10.1128/genomeA.00879-15

45 Lyons, E., Freeling, M., Kustu, S. & Inwood, W. Using Genomic Sequencing for Classical Genetics in E. coli K12. *PloS one* **6**, e16717 (2011). https://doi.org:10.1371/journal.pone.0016717

46 Soupene, E. *et al.* Physiological studies of Escherichia coli strain MG1655: growth defects and apparent cross-regulation of gene expression. *J Bacteriol* **185**, 5611-5626 (2003).

47 Le, D. *et al.* Active Efflux Leads to Heterogeneous Dissipation of Proton Motive Force by Protonophores in Bacteria. *mBio* **12**, e00676-00621 (2021). https://doi.org:doi:10.1128/mBio.00676-21

48 Le, D., Akiyama, T., Weiss, D. & Kim, M. Dissociation kinetics of small-molecule inhibitors in Escherichia coli is coupled to physiological state of cells. *Communications Biology* **6**, 223 (2023). https://doi.org:10.1038/s42003-023-04604-9

49 Dawson, E., Şimşek, E. & Kim, M. in *Bacterial Persistence: Methods and Protocols* (eds Natalie Verstraeten & Jan Michiels) 85-93 (Springer US, 2021).

50 Ershov, D. *et al.* TrackMate 7: integrating state-of-the-art segmentation algorithms into tracking pipelines. *Nature Methods* **19**, 829-832 (2022). https://doi.org:10.1038/s41592-022-01507-1

51 Zahir, T. *et al.* High-throughput time-resolved morphology screening in bacteria reveals phenotypic responses to antibiotics. *Communications Biology* **2**, 269 (2019). https://doi.org:10.1038/s42003-019-0480-9

52 Miller, G. in *Information theory in Psychology II-B* p95-100 (Free Press,, 1955).

Figure 1

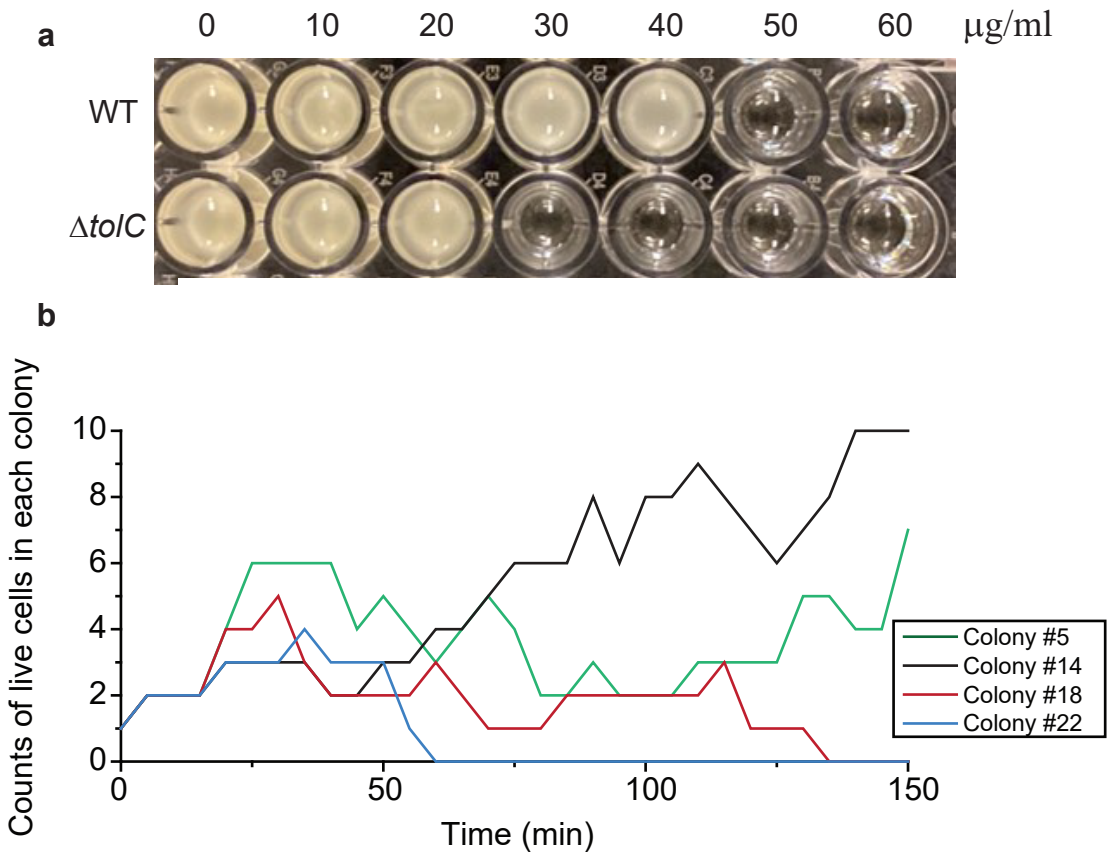
a
0
10
20
30
40
50
60
μg/ml
WT
ΔtolC
b
Counts of live cells in each colony
Time (min)
Colony #5
Colony #14
Colony #18
Colony #22

Figure 2

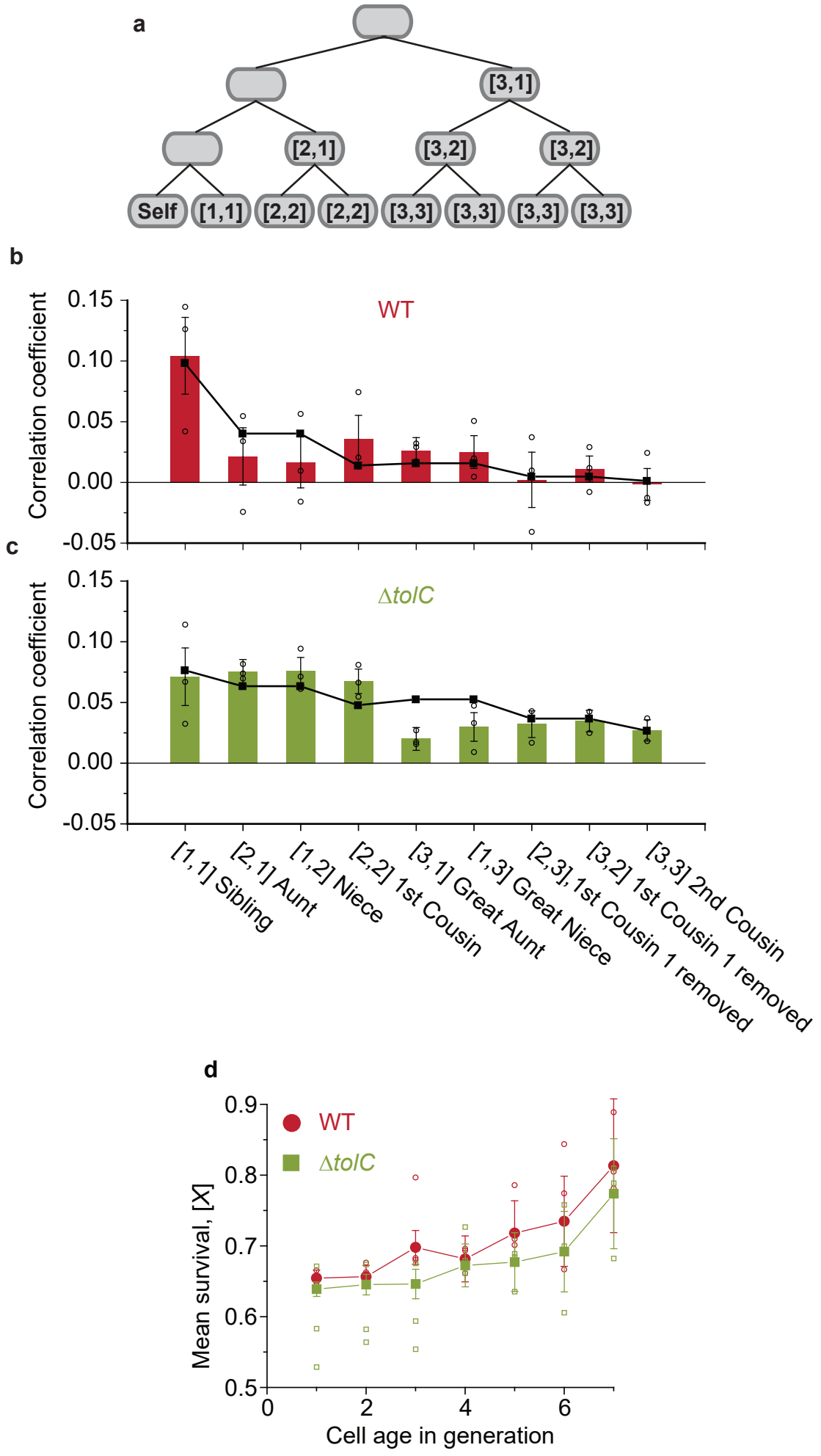
a
[3,1]
[2,1]
[3,2]
[3,2]
Self
[1,1]
[2,2]
[2,2]
[3,3]
[3,3]
[3,3]
[3,3]
b
WT
Correlation coefficient
0.15
0.10
0.05
0.00
-0.05
c
ΔtolC
Correlation coefficient
0.15
0.10
0.05
0.00
-0.05
[1,1] Sibling
[2,1] Aunt
[1,2] Niece
[2,2] 1st Cousin
[3,1] Great Aunt
[1,3] Great Niece
[2,3] 1st Cousin 1 removed
[3,2] 1st Cousin 1 removed
[3,3] 2nd Cousin
d
WT
ΔtolC
Mean survival, [X]
0.9
0.8
0.7
0.6
0.5
0
2
4
6
Cell age in generation

Figure 3

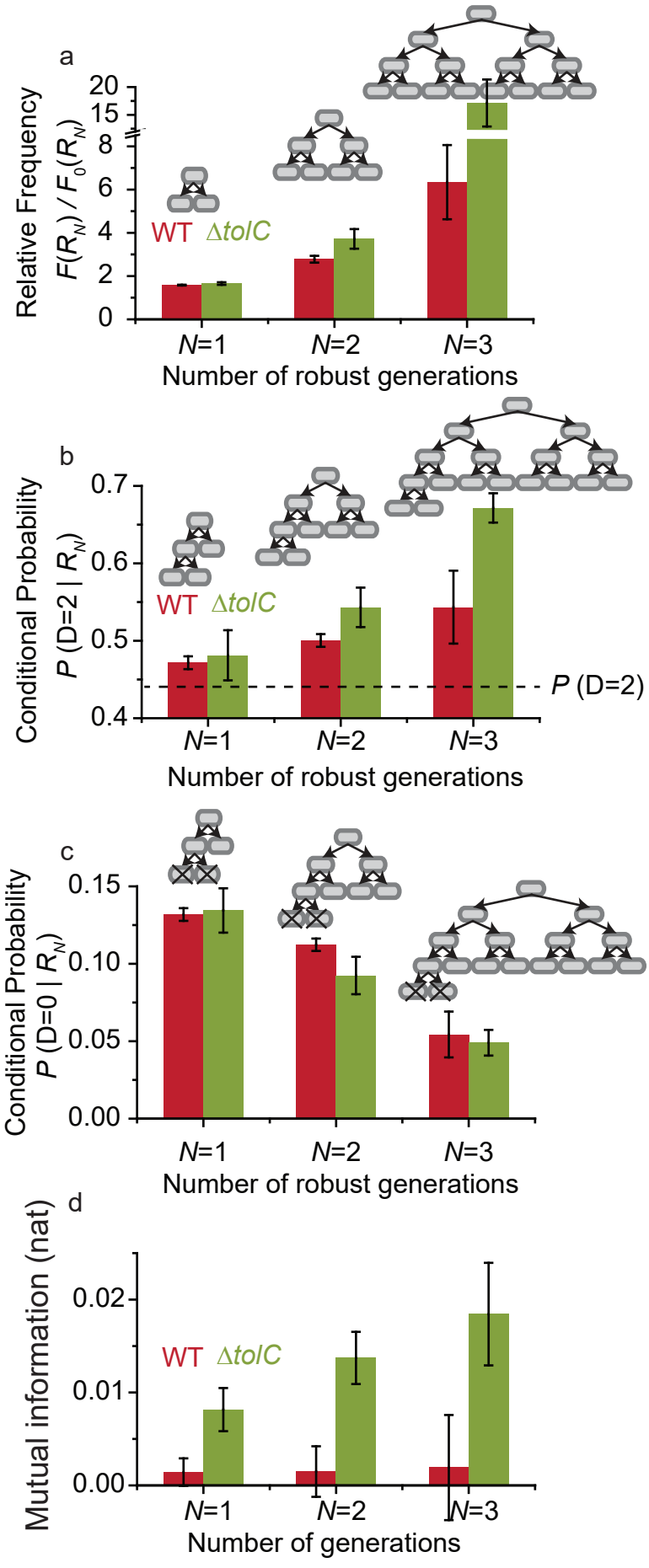
a
Relative Frequency
$F(R_N) / F_0(R_N)$
20
15
8
6
4
2
0
WT
ΔtolC
N=1
N=2
N=3
Number of robust generations
b
Conditional Probability
P (D=2 | R_N)
0.7
0.6
0.5
0.4
WT
ΔtolC
P (D=2)
N=1
N=2
N=3
Number of robust generations
c
Conditional Probability
P (D=0 | R_N)
0.15
0.10
0.05
0.00
N=1
N=2
N=3
Number of robust generations
d
Mutual information (nat)
0.02
0.01
0.00
WT
ΔtolC
N=1
N=2
N=3
Number of generations

Figure 4

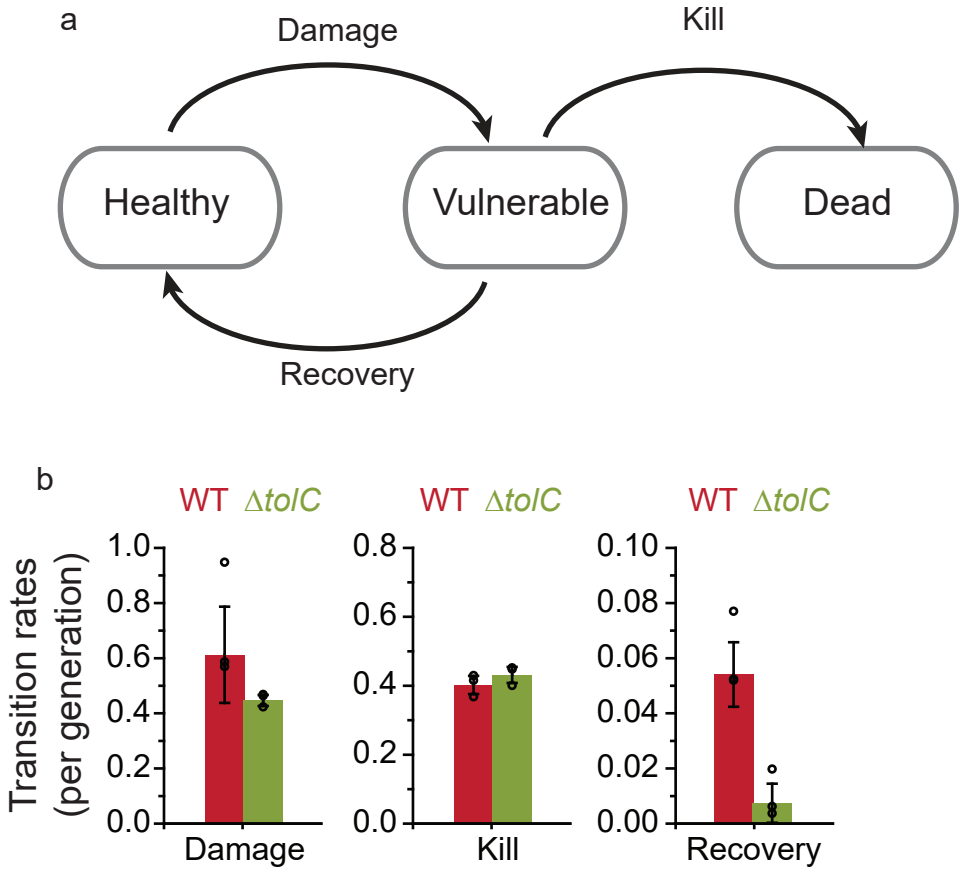
a
Damage
Kill
Healthy
Vulnerable
Dead
Recovery
b
WT ΔtolC
WT ΔtolC
WT ΔtolC
Transition rates (per generation)
1.0
0.8
0.6
0.4
0.2
0.0
0.8
0.6
0.4
0.2
0.0
0.10
0.08
0.06
0.04
0.02
0.00
Damage
Kill
Recovery